Numerical and laboratory investigation of breaking of steep two-dimensional waves in deep water

ALEXANDER V. BABANIN[1]†, **DMITRY CHALIKOV**[1,2]
I. R. YOUNG[1] **AND IVAN SAVELYEV**[3]

[1]Swinburne University of Technology, Melbourne, Victoria 3122, Australia
[2]P.P. Shirshov Institute of Oceanology, Maly Pr. V. I. Saint-Petersburg 199053, Russia
[3]RSMAS, University of Miami, FL 33149, USA

The paper extends a pilot study into a detailed investigation of properties of breaking waves and processes responsible for breaking. Simulations of evolution of steep to very steep waves to the point of breaking are undertaken by means of the fully nonlinear Chalikov–Sheinin model. Particular attention is paid to evolution of nonlinear wave properties, such as steepness, skewness and asymmetry, in the physical, rather than Fourier space, and to their interplay leading to the onset of breaking. The role of superimposed wind is also investigated. The capacity of the wind to affect the breaking onset is minimal unless the wind forcing is very strong. Wind is, however, important as a source of energy for amplification of the wave steepness and ultimately altering the breaking statistics. A detailed laboratory study is subsequently described. The theoretical predictions are verified and quantified. In addition, some features of the nonlinear development not revealed by the model (i.e. reduction of the wave period which further promotes an increase in steepness prior to breaking) are investigated. Physical properties of the incipient breaker are measured and examined, as well as characteristics of waves both preceding and following the breaker. The experiments were performed both with and without a superimposed wind, the role of which is also investigated. Since these idealized two-dimensional results are ultimately intended for field applications, tentative comparisons with known field data are considered. Limitations which the modulational instability mechanism can encounter in real broadband three-dimensional environments are highlighted. Also, substantial examination of existing methods of breaking onset detection are discussed and inconsistencies of existing measurements of breaking rates are pointed out.

1. Introduction

The breaking of deep-water surface waves represents an interesting and challenging problem of fluid mechanics. Such breaking is a strongly nonlinear intermittent random process, very rapid compared to other processes in the system of surface waves in general and wind-generated waves in particular. The distribution of breaking on the water surface is not continuous, but its role in maintaining the energy balance

† Email address for correspondence: ABabanin@groupwise.swin.edu.au

within the continuous wind-wave field is critical. Despite the significant research effort devoted to the subject in the past decades, a compelling physical understanding and mathematical description of the phenomenon remain elusive.

Ocean wave breaking plays the primary role in air–sea exchange of momentum, mass and heat, and constitutes the major element of one of the most significant mechanisms which drive wave evolution – wave energy dissipation. It is also of importance for ocean remote sensing, coastal and maritime engineering, navigation and other practical applications.

In this paper, we will be mostly interested in hydrodynamic rather than air–sea interaction aspects of wave breaking. Waves are known to break even in the total absence of wind forcing, provided hydrodynamic conditions are appropriate (e.g. Melville 1982; Rapp & Melville 1990; Babanin *et al.* 2007*b*). Why and when will such breaking occur? Breaking waves are not only steep but have been found also to exhibit such distinct nonlinear features as vertical and horizontal asymmetries (e.g. Caulliez 2002; Young & Babanin 2006), some of which cannot be reproduced by perturbation theories. Therefore, fully nonlinear theories have to be employed in the search for mechanisms leading to breaking onset.

Beyond the point of onset, breaking occurs very rapidly, lasting only a fraction of the wave period (Rapp & Melville 1990), but the wave may lose more than a half of its height (Liu & Babanin 2004). Thus, the wave energy that slowly accumulated under wind action over hundreds of wave periods is suddenly released in the space of less than one period. Conceptually, however, the process of wave collapse is different from the processes leading to breaking onset and should be considered separately. It will not be the focus of the present paper.

Intermittency is another distinct difference between breaking and other mechanisms involved in wave evolution. It is only under very strong winds that the percentage of breaking crests in a time series can reach 50 % or more. Normally it is well below 10 % (Babanin, Young & Banner 2001). This intermittent process is, however, still sufficient to balance the continuous process of wind input and nonlinear evolution.

As stated above, breaking is primarily a hydrodynamic process. While the effect of a breaking event on the instantaneous wind input can be very significant (Babanin *et al.* 2007*a*), the very large density difference between the air and the water means that instantaneously the wind can only play a minor role in determining breaking onset and the subsequent breaking progress. As instantaneous, we mean the time scale of the order of one period, at which the breaking happens. On the longer time scale of hundreds of wave periods, however, the role of the wind is very important in increasing, albeit slowly, wave steepness (nonlinearity) which can then lead to wave breaking. The wind also appears to play a role in altering wave modulation properties and subsequent energy loss due to wave breaking. These multiple roles of wind forcing will also be discussed in the paper.

This paper extends our pilot numerical/laboratory study of wave breaking onset (Babanin *et al.* 2007*b*). As outlined in Babanin *et al.* (2007*b*), the topic is not new and over the last 30 years, theoretical (e.g. Longuet-Higgins & Cokelet 1978), experimental (e.g. Melville 1982) and numerical (e.g. Dold & Peregrine 1986) approaches have been applied to investigate instability mechanisms active in nonlinear wave fields, which lead to wave breaking. These mechanisms relate to the Benjamin–Feir-like (BF) instability (Benjamin & Feir 1967) which controls the modulation of trains of weakly nonlinear waves, and as a result, some waves can become very large and ultimately break (e.g. Chalikov 2007).

This study is done in terms of free-surface wave properties in physical rather than Fourier space. We do not rely on existence of wave groups (sidebands) in the initial wave field because the formation of the appropriate wave groups accompanying wave breaking is an internal process in the nonlinear wave field subject to physical instabilities. Rather, our initial conditions consist of steep monochromatic waves which are allowed to evolve and this evolution appears to inevitably lead to breaking if the initial waves are sufficiently steep. Sidebands naturally grow from the background noise and are expected to be defined by the ratio of characteristic wave steepness $\epsilon = ak_0$ to spectral bandwidth $\Delta\omega/\omega_0$, where k_0 and ω_0 are some characteristic wavenumber and angular frequency respectively, and a is the mean amplitude at this wavenumber:

$$M_I = \frac{\epsilon}{\Delta\omega/\omega_0}. \tag{1.1}$$

This ratio was shown important in the original studies of instabilities of weakly modulated trains of monochromatic carrier waves of small amplitudes. Here, we denote this ratio as M_I (modulational index). Our study mainly deals with slowly modulated two-dimensional monochromatic waves, which are, however, even initially not of the small amplitude, and therefore, analogy of the observed empirical modulational interplay with the small-amplitude near-monochromatic theoretical BF process should be treated with caution. In our paper, M_I signifies the fact that the wave steepness and length of wave modulation (or number N of waves in the modulation where $1/N \sim \Delta k/k_0$) are not independent quantities, i.e. steeper waves will correspond to fewer waves in a modulation. Thus, if nonlinear monochromatic waves are allowed to evolve, they will form groups where N is not a free parameter, but will be defined by the initial steepness ϵ.

In Babanin *et al.* (2007*b*), prediction of the breaking onset of two-dimensional waves in deep water was attempted first by means of a fully nonlinear numerical model and then tested in a laboratory experiment. Distance to the point of breaking could be controlled by varying the initial monocromatic steepness (IMS) ϵ_0. Thus, the incipient breaker was measured and found to asymptote at the Stokes steepness limit of $2\epsilon_{br} \approx 0.88$.

This paper extends the pilot study into a detailed investigation of the properties of breaking waves and the processes responsible for breaking. In §2 of the present paper, simulations of the evolution of steep to very steep waves to the point of breaking are undertaken by means of the fully nonlinear Chalikov–Sheinin model (Chalikov & Sheinin 2005). Particular attention is paid to the evolution of nonlinear wave properties, such as steepness, skewness and asymmetry, and to their interplay leading to the onset of breaking. The role of the superimposed wind is also mentioned.

In §3, the detailed laboratory study is described. The theoretical predictions are verified and quantified. In addition, some features of the nonlinear development not revealed by the model (i.e. reduction of the wave period which further promotes an increase in steepness prior to breaking) are investigated. Since the location of the incipient breaker can be controlled, its physical properties are examined as well as characteristics of waves both preceding and following the breaker. The experiments were performed both with and without a superimposed wind, the role of which is also investigated.

Since these idealized two-dimensional results are ultimately intended for field applications, in §4, tentative comparisons with known field data are considered. Limitations which the BF mechanism can encounter in real broadband three-dimensional environments (e.g. Brown & Jensen 2001; Onorato, Osborne & Serio

2002) are highlighted. Also, existing methods of breaking onset detection are discussed and the inconsistencies of existing measurements of breaking rates are pointed out. Finally, overall conclusions of the study are summarized.

2. Numerical simulations

Numerical computations of nonlinear surface waves have previously been undertaken based on solutions of the potential flow equations (e.g. Watson & West 1975; Longuet-Higgins & Cokelet 1976; West, Brueckner & Janda 1987) and with a Cauchy-type integral algorithm (Dold 1992). Both schemes have no limitation in terms of wave steepness, and both were capable of simulating the initial phase of wave breaking (the later stages are rotational and remain extremely difficult to simulate directly). More recently, a method based on a Taylor expansion of the Dirichlet–Neumann operator was developed by Craig & Sulem (1993). Capabilities of this method were illustrated by computing the evolution of modulated wave packets and a low-order approximation of a Stokes wave for relatively short periods of time. We should point out that this appears to be a principle limitation of all the above schemes: for a steep wave field, they have only been used for simulations of relatively short time/space evolution.

A numerical scheme for direct hydrodynamic modelling of one-dimensional nonlinear gravity and gravity–capillary waves was developed by Chalikov & Sheinin (1998) (see also Chalikov 2005, 2007; Chalikov & Sheinin 2005). This approach is based on a non-stationary conformal mapping, which allows the equations of potential flow with the inclusion of a free surface to be written in a surface-following coordinate system. This transformation does not impose any restrictions on the shape of the surface, except that it has to be possible to represent this surface in terms of a Fourier series.

Let us consider periodic one-dimensional deep-water waves whose dynamics is described by principal potential equations. Due to the periodicity condition, the conformal mapping for infinite depth can be represented by the Fourier series (see details in Chalikov & Sheinin 1998, 2005):

$$x = \xi + \sum_{-M \leqslant k < M, k \neq 0} \eta_{-k}(\tau) \exp(k\zeta) \, \vartheta_k(\xi), \qquad (2.1)$$

$$z = \zeta + \sum_{-M \leqslant k < M, k \neq 0} \eta_k(\tau) \exp(k\zeta) \, \vartheta_k(\xi), \qquad (2.2)$$

where x and z are Cartesian coordinates, ξ and ζ are conformal surface-following coordinates, τ is time, η_k are coefficients of the Fourier expansion of free surface $\eta(\zeta, \tau)$ with respect to the new horizontal coordinate ζ:

$$\eta(\zeta, \tau) = h\left(x(\zeta, \xi = 0, \tau), t = \tau\right) = \sum_{-M \leqslant k \leqslant M} \eta_k(\tau) \, \vartheta_k(\zeta), \qquad (2.3)$$

ϑ_k denotes the functions

$$\vartheta_k(\xi) = \begin{cases} \cos k\xi & \text{for } k \geqslant 0, \\ \sin k\xi & \text{for } k < 0 \end{cases} \qquad (2.4)$$

and M is truncation number.

Nontraditional presentation of the Fourier transform with the definition (2.4) is, in fact, more convenient for computations with real numbers, such as $(\vartheta_k)_\xi = k\vartheta_{-k}$ and

$\sum(A_k \vartheta_k)_\xi = -\sum k A_{-k} \vartheta_k$. So, the Fourier coefficients A_k form a real array $A(-M : M)$, thus making possible a compact programming in Fortran 90. Such presentation can be generalized for two-dimensional case.

Note that the definition of both coordinates ξ and ζ is based on Fourier coefficients for surface elevation. It then follows from (2.1) and (2.2) that time derivatives z_τ and x_τ for Fourier components are connected by a simple relation:

$$(x_\tau)_k = \begin{cases} -(z_\tau)_{-k} & \text{for } k > 0, \\ (z_\tau)_k & \text{for } k < 0. \end{cases} \tag{2.5}$$

Due to conformity, the Laplace equation retains its form in (ξ, ζ) coordinates. It is shown in Chalikov & Sheinin (1998, 2005) that the potential wave equations can be represented in the new coordinates as follows:

$$\Phi_{\xi\xi} + \Phi_{\zeta\zeta} = 0, \tag{2.6}$$

$$z_\tau = x_\xi G + z_\zeta F, \tag{2.7}$$

$$\Phi_\tau = F\Phi_\xi - \frac{1}{2}J^{-1}\left(\Phi_\xi^2 - \Phi_\zeta^2\right) - z, \tag{2.8}$$

where (2.7) and (2.8) are written for the surface $\zeta = 0$ (so that $z = \eta$, i.e. the surface elevation), J is the Jacobian of the transformation:

$$J = x_\xi^2 + z_\xi^2 = x_\zeta^2 + z_\zeta^2, \tag{2.9}$$

G is an auxuliary function:

$$G = (J^{-1}\Phi_\zeta)_{\zeta=0} \tag{2.10}$$

and F is a generalization of the Hilbert transform of G, which for $k \neq 0$ may be defined in Fourier space as

$$G_k = \begin{cases} -F_{-k} & \text{for } k > 0, \\ F_k & \text{for } k < 0, \end{cases} \tag{2.11}$$

actually following from (2.5). Above, Φ is the velocity potential (and Φ_ζ is the derivative of the potential with respect to the 'vertical' coordinate ζ at the surface), z represents the shape of the surface.

Equations (2.6)–(2.11) are written in non-dimensional form with the following scales: length L, where $2\pi/L$ is the (dimensional) horizontal wavenumber, time $L^{1/2}g^{-1/2}$ and the velocity potential $L^{3/2}g^{-1/2}$ (g is the acceleration of gravity). Capillary effects and external pressure were not taken into account in this investigation. Note that the adiabatic equations for surface waves outside the capillary interval are self-similar: they are invariant over length scale L, and this makes the numerical approach very effective and allows broad interpretations of laboratory experiments.

The boundary condition assumes vanishing vertical velocity at infinite depth

$$\Phi_\zeta(\xi, \zeta \to -\infty, \tau) = 0. \tag{2.12}$$

Solution of the Laplace equation (2.6) with boundary condition (2.12) yields to Fourier expansion which reduces the system (2.6)–(2.8) to a one-dimensional problem:

$$\Phi = \sum_{-M \leqslant k \leqslant M} \phi_k(\tau) \exp(k\zeta) \vartheta_k(\xi), \tag{2.13}$$

where ϕ_k are Fourier coefficients of the surface potential $\Phi(\xi, \zeta = 0, \tau)$. Equations (2.6)–(2.8), (2.10) and (2.11) constitute a closed system of prognostic equations

for the surface functions $z(\xi, \zeta = 0, \tau) = \eta(\xi, \tau)$ and the surface velocity potential $\Phi(\xi, \zeta = 0, \tau)$. For more detailed descriptions of the analytical and numerical model, we refer to Chalikov & Sheinin (1998, 2005).

Remarkably, this new formulation is also simpler than the original set of equations since the nonlinear conformal coordinate transformation removes a number of nonlinear terms. For the stationary case, this method coincides with the classical complex variable method, e.g. Crapper (1957), and an efficient numerical scheme (CS) for this was developed by Chalikov & Sheinin (1998). Note that this scheme is more precise than the popular surface integral scheme (Dold 1992). In addition, compared to the CS scheme, the surface integral method is too complicated: a complete set of its equations occupy several pages. For the CS scheme, the equations take three lines and the core of the numeric scheme takes 11 lines in Fortran 90.

The accuracy of this scheme was demonstrated by a long-term simulation of very steep Stokes waves ($ak = 0.42$). The stability of Stokes waves has been a subject of significant speculations. In the CS case, 11 decimal places of precision and a fourth-order Runge–Kutta scheme were sufficient to simulate the propagation of a virtually undisturbed Stokes wave for up to 1000 periods.

The conformal mapping even made it possible to reproduce the initial stages of the breaking process where the surface ceases to be a single-valued function. Thus, the CS scheme has a number of important advantages: (i) comparison with an exact solution showed that the scheme has extremely high accuracy; (ii) it preserves integral invariants; (iii) it is very efficient: its computation time scales as $M \log(M)$ where M is the number of modes, whereas the Dold scheme scales as as M^2; (iv) the scheme demonstrates stability over millions of time steps (thousands of periods of the dominant wave). This scheme is able to reproduce a nonlinear concentration of energy in physical space resulting in wave breaking and potentially in the appearance of freak waves.

In the CS model, the wave model is coupled with an atmospheric boundary layer model:

$$\Phi_\tau = F\Phi_\xi - \frac{1}{2}J^{-1}\left(\Phi_\xi^2 - \Phi_\zeta^2\right) - z - p, \qquad (2.14)$$

where p is a surface pressure, which describes exchange of momentum and energy between the air and water. In the present investigation, in order to speed up the computations, the coupling was conducted by means of a β-function which parameterized the connection of the surface pressure and the surface shape on the basis of an exhaustive set of numerical simulations by means of the coupled model. Real and imaginary Fourier amplitudes of pressure p_r and p_i are calculated as linear function of amplitudes of water elevation η_r and η_i:

$$p_r + \mathrm{i}p_i = (\beta_r + \mathrm{i}\beta_i)(\eta_r + \mathrm{i}\eta_i). \qquad (2.15)$$

The real and imaginary parts of this β-function are functions of non-dimensional frequency $\Omega = u(l_k/2)\omega$ where $u(l_k/2)$ is wind velocity at height equal to half of wavelength l_k, $\omega = |k|^{1/2}$ (both ω and k are non-dimensional variables). Thus, it is possible to introduce wind forcing of the waves. This option will be actively employed in our study.

2.1. *Testing the Chalikov–Sheinin model*

For the purposes of the present study, the model's ability to reproduce wave evolution without limitations in terms of steepness or duration of propagation is crucial. For this reason, the CS model was chosen for the detailed numerical simulations of physical
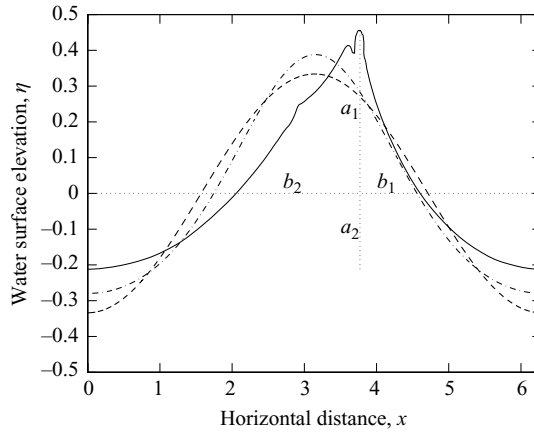
FIGURE 1. Geometric definition of wave skewness and asymmetry. The wave propagates from left to right. Solid line: numerically simulated incipient breaker; dashed line: harmonic wave; dash-dotted line: Stokes wave. Dotted lines are the mean (zero) water level (horizontal) and the line drawn from the breaker crest down to the level of its trough (vertical).

characteristics of strongly nonlinear waves leading to the onset of breaking. Before being employed in the present study, the CS model had previously been extensively verified and tested (Chalikov & Sheinin 1998, 2005) and used in a number of strongly nonlinear applications (e.g. Chalikov 2005, 2007). It was now additionally checked in terms of its capacity to model nonlinear wave features associated with wave breaking.

One of early motivations for the present study was to search for a theory able to describe wave asymmetry with respect to the vertical axis. Definitions of the asymmetry and skewness are given in figure 1, reproduced with modifications from Babanin *et al.* (2007*b*). In mathematical terms, these definitions are

$$A_s = \frac{b_1}{b_2} - 1, \quad S_k = \frac{a_1}{a_2} - 1. \quad (2.16)$$

Thus, positive skewness represents a crest sharper than the trough and negative asymmetry represents a wave tilted forwards.

Intrinsically, both the asymmetry and the skewness are natural features of steep deep-water waves regardless of their size, crest length, forcing or generation source. Importantly for this study, experimentally observed asymmetry A_s has been broadly associated with the wave breaking (e.g. Caulliez 2002; Young & Babanin 2006). Perturbation theories cannot reproduce such asymmetry for deep-water waves, and therefore, since we intended to study physical features of near-breaking waves, a fully nonlinear theory was obviously required. Figure 1 illustrates the capacity of the CS model in this regard. In the figure, three types of waves of the same height and length, i.e. of the same mean steepness, are shown. Once the skewness is non-zero and the amplitude a is not clearly defined, a definition of the wave steepness in terms of ak becomes ambiguous. Therefore, unless otherwise specified, the steepness will be expressed in terms of wave height $H = a_1 + a_2$ rather than wave amplitude a, as $\epsilon = Hk/2$. In these terms, a steepness $\epsilon = 0.335$ of the wave shown in the figure far exceeds the limits of a perturbation analysis.

The dashed line in figure 1 represents a steep sinusoidal wave ($S_k = A_s = 0$). Such a wave will immediately transform itself into a Stokes wave (e.g. Chalikov & Sheinin 2005), an example of which is shown in the figure by the dash-dotted line. This steep

Stokes wave is highly skewed ($S_k = 0.39$), but remains symmetric (i.e. $A_s = 0$). The incipient breaker in figure 1 (solid line, $S_k = 1.15$, $A_s = -0.51$) was produced by the CS model, in a simulation which commenced with an initially monochromatic wave of $IMS = 0.25$ (initial monochromatic steepness). Such a wave profile visually looks realistic for a breaker and corresponds to, or even exceeds, experimental values of skewness and asymmetry for breaking waves previously observed (e.g. up to $A_s = -0.5$ instantaneously in Caulliez 2002 or $A_s = -0.2$ on average in Young & Babanin 2006). It is worth noting that the steepness of the individual wave has grown very significantly at the point of the breaking: from $IMS = 0.25$ to $\epsilon = 0.335$. Result shown in figure 1 was obtained for initially assigned harmonic wave at wavenumber $k = 1$ and number of modes $M = 1024$. All other computations described below were conducted for an harmonic wave assigned at $k = 16$ and number of modes $M = 2048$.

Disturbance seen at the crest of the incipient breaker in figure 1 has to be mentioned. For waves of very high steepness, instabilities of the local flow near wave crest, which are different from instabilities of the whole wave, are known to develop (e.g. Longuet-Higgins & Dommermuth 1997). Thus, the CS model is not only capable of producing realistic values of the asymmetry, typically associated with the breaking experimentally, but even demonstrates crest instabilities expected theoretically.

2.2. *Simulating the evolution of nonlinear waves to breaking*

In the numerical simulations, a wave is regarded as breaking if the water surface becomes vertical at any point. Criterion for terminating the model run was defined by the first appearance of a non-single value of surface in the interval $x = (0, L)$:

$$x(i + 1) < x(i), i = 1, 2, 3, \ldots, N - 1, \tag{2.17}$$

where N is the number of points on the wave profile over its length L.

We will concentrate on three physical properties: wave steepness, skewness and asymmetry and their inter-relationships. We will then try to reproduce and investigate these properties in a laboratory experiment with two-dimensional waves. If these properties are indeed linked to wave breaking, but the percentage of breaking waves is small, as it usually is (see §1), then examination of average steepness, skewness or asymmetry is likely to be of little use. Therefore, the majority of our analysis will concentrate on nonlinear properties of individual waves.

Figure 2 shows the simulated evolution of the nonlinear wave properties to the point of breaking in the presence of wind forcing. The wind forcing is expressed in terms of ratio U/c where U is the wind speed and c is the phase speed of the wave with wavenumber k. Three sets of subplots correspond to three wind-forcing conditions: $U/c = 2.5$ (moderate forcing), $U/c = 5.0$ (strong forcing) and $U/c = 10.0$ (very strong forcing). The initial steepness chosen is $IMS = 0.26$, which should lead to a fast evolution to breaking onset.

The period of the modulation of all the nonlinear properties shown is equal to twice the wave period. While the maxima of instantaneous steepness keep growing, the skewness and asymmetry oscillate without a noticeable increase in magnitude. Thus, it can be concluded that it is some critical value of local steepness which defines the breaking.

Figure 2(*a–c*) corresponds to a moderate wind-forcing condition of $U/c = 2.5$. The maximum of instantaneous steepness keep growing and reach a value of $\epsilon = 0.34$ at the point which is interpreted as incipient breaking by the model. Figure 2(*d–f*) corresponds to much stronger wind forcing of $U/c = 5.0$. Apart from the faster steepness growth, almost all the other properties of the nonlinear evolution remain
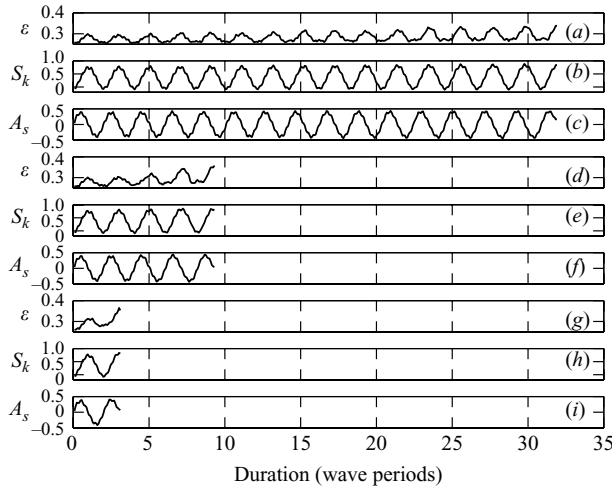
FIGURE 2. Simulations of steepness (*a*, *d*, *g*), skewness (*b*, *e*, *h*), asymmetry (*c*, *f*, *i*) of the wave of *IMS* = 0.26 as it evolves from the initial conditions to the point of breaking. The values of U/c are 2.5 (*a–c*), 5.0 (*d–f*) and 10.0 (*g–i*). The *x*-axis shown at the bottom remains the same for all.

similar to the previous test. Steepness ($\epsilon = 0.36$) and skewness ($S_k = 0.82$) values at breaking are close to those of the above test, asymmetry at breaking approaches zero.

It is interesting to note that, according to known results on the wave amplification by wind, the wave growth increment at non-extreme conditions should be approximately a quadratic function of the wind (e.g. Donelan *et al.* 2006). If indeed there is some critical steepness signifying the breaking onset, then doubling of the wind speed in our numerical tests should lead to this limiting value being reached four times faster. This conjecture produces a result close to that simulated: the duration of the evolution to breaking has now been reduced from 32 to 9 wave periods (almost 4 times).

A further doubling of the wind input, as shown in figure 2(*g–i*), led to another reduction of the evolution duration – from nine to three periods. This is again consistent with Donelan *et al.* (2006) who showed that at very strong winds the relative wave growth actually slows down. The other patterns of the wave nonlinear evolution appear unaltered, the maximum values of steepness $\epsilon = 0.36$ and skewness $S_k = 0.83$ are almost similar to the previous case. These values also demonstrate that the instantaneous effect of the wind on the breaking onset is negligible as the wind forcing of $U/c = 10.0$ is now very strong.

The oscillations of asymmetry are shifted in phase with respect to steepness and skewness. The asymmetry oscillates about zero in the range ± 0.45 which means that the waves are periodically tilted backwards and forwards. If the point of maximum steepness (skewness) is passed without breaking, the asymmetry becomes negative, i.e. the wave begins to lean forwards. If this point signifies the breaking onset, the wave still apparently continues to tilt forwards, and this explains why all the breaking waves exhibit negative asymmetry. In these simulations, the negative asymmetry does not appear to be an indication of the breaking but is rather an indication of the modulation phase at which breaking-in-progress may or may not occur.

Figure 3 shows a composite set of fetch-versus-steepness dependences for different values of wind forcing $U/c = 1$–11. The fetch is expressed in dimensionless terms of number of wavelengths (wave periods) to the breaking at a particular *IMS*. Figure 3
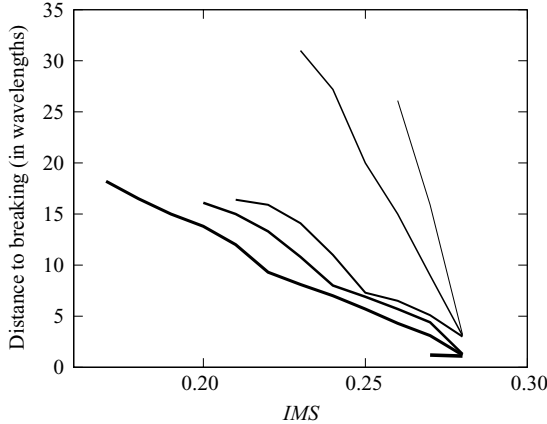
FIGURE 3. Numerical simulations, number of wavelengths to the breaking versus $IMS = ak$, different wind forcing of $U/c = 1, 3, 7.5, 8, 8.5, 11$ is shown with progressively thickening lines.

allows the estimation, based on the numerical simulations with the CS model, of when a two-dimensional wave breaks. As it will be shown in §3, quantitative application of these numerical results to laboratory waves may be limited, but qualitatively this picture agrees well with the experiment.

2.3. *Influence of wind and initial steepness*

The role of the wind in the wave breaking has already been mentioned (see also Waseda & Tulin 1999, for a discussion of the wind influence on the modulational instability). It is apparently very important in growing the wave steepness (i.e. figures 2 and 3). In this section, we will discuss the capacity of the wind to affect the breaking onset, i.e. can the wind push a steep wave over and thus reduce the limiting steepness at breaking?

Due to the very large density difference between the water and the air, such a possibility seems unlikely (e.g. figure 2). In figure 4, the nonlinear features of the incipient breaker are shown as a function of IMS for a variety of wind-forcing conditions. The simulations were run for a limited number of wave periods and some waves may not break (e.g. for $U/c = 3$, the waves do not have enough time to break if $IMS < 0.25$).

In figure 4(a), the limiting steepness at breaking onset is plotted for $U/c = 3$ (dotted line), 5 (dashed line), 8 (dash-dotted line) and 11 (solid line). The incipient breaking steepness actually grows, rather than being reduced, with stronger wind forcing. Even though the growth is marginal, the four lines clearly separate and therefore instantaneous steepness at breaking appears to be somewhat larger at stronger winds. The skewness and asymmetry of the incipient breakers (figures 4b and 4c) do not depend on wind except at the extreme wind forcing of $U/c = 11$. Thus, it is only at extreme conditions that the wind is capable of influencing the wave shape at breaking, and even then the effect is marginal.

3. Laboratory experiment

To begin this section, it should be emphasized that comparisons of the numerical simulations of nonlinear wave evolution described above with the laboratory experiments in this section can only be qualitative. Firstly, no matter how sophisticated
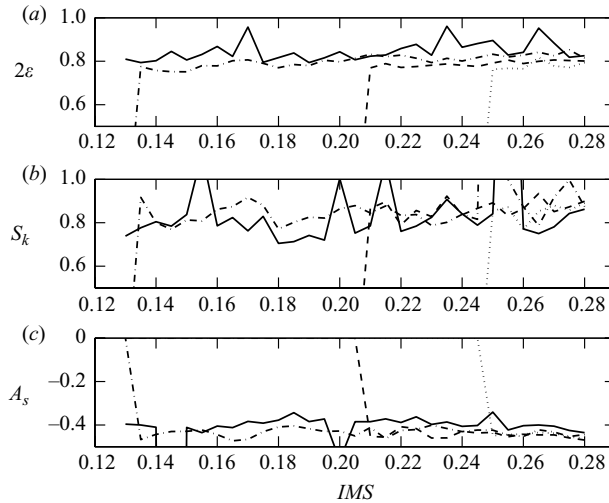
FIGURE 4. The influence of wind on the nonlinear properties of incipient breakers. (*a*) Steepness; (*b*) skewness; (*c*) asymmetry versus *IMS* for $U/c = 3$ (dotted line), 5 (dashed line), 8 (dash-dotted line) and 11 (solid line).

the model is, it is still a simplification of the physical environment and disregards or possibly suppresses some natural features. One of such features is the three-dimensionality of wave motion. Even in the quasi-two-dimensional environment of the wave tank, some directional features may still play an essential role. For example, Melville (1982) showed that at steepness $\epsilon > 0.3$ the wave crests develop a crescent-shaped perturbation and such wave behaves in a more complicated way compared to the strictly two-dimensional BF case. This has a significant consequence for our simulations. The two-dimensional CS model predicts immediate breaking onset for $\epsilon > 0.29$ whereas in the laboratory experiments of Melville (1982) such waves become short crested but can persist without breaking for some time.

Another significant difference between the laboratory and model is the continuous nature of modes in the experimental environment, even if those modes are only minor background noise, and the discrete nature of numerical modes. It is important to understand that at the initial stages of development, the necessary modes, defined by M_I (1.1), should grow from the continuous noise. These modes, however, can be suppressed or even removed completely in a discretized numerical model. In such a circumstance, the waves, even if they are steep Stokes waves, will propagate for an indefinitely long period without breaking, as was described in §2.

If the model is constructed so as to allow multiple modes, another numerical feature still distinguishes the model from nature. The background noise, the source of the necessary modes dictated by M_I, cannot be completely reduced to zero in nature. In a digitized medium it can, however, be made very small. For example, in the CS numeric scheme, the eleventh-order decimal accuracy is employed. Such accuracy is essential for precise simulations, but since it is the only source of noise in the system, it can obviously slow down the development of the initial BF modes. As is sometimes done in numerical simulations (e.g. Dold & Peregrine 1986), the modes can be deliberately introduced as initial conditions. Such an approach was not, however, employed in the present study, since in this scenario M_I of the system is pre-defined, and wave development to breaking may be altered.

The model has obvious limitations in simulating the final stages of incipient breaking and in our simulations it was stopped when the water surface became vertical at any point. Strictly speaking, this geometrical property of the surface can be used as a physical definition of the breaking onset. In the numerical simulations it was noticed that the local steepness can be very large, but the carrier wave can still recover to a non-breaking state. If, however, a negative slope appears locally, the wave never returns to a non-breaking scenario because the water volume intersecting the vertical line tends to collapse. Apparently, the same considerations are applicable to the physical waves too.

At present, the concept of incipient breaking or breaking onset is poorly defined and even ambiguous. Traditionally, the initial phases of a breaker-in-progress are treated as incipient breaking. In Caulliez (2002), for example, surface elevations were recorded, differentiated, and the wave was regarded as a 'near-breaker' if its slope exceeded 0.586 anytime between two subsequent zero-downcrossings. This criterion is an estimate of the highest slope which a Stokes wave can reach (Longuet-Higgins & Fox 1977). But if this slope is exceeded, then the wave is already breaking. This is not an incipient breaker, but represents breaking in progress. Features and physics of breaking-in-progress, however, may be very different to that of incipient breaking. Thus, investigation of geometric, kinematic, dynamic and other properties of breaking-in-progress, such as whitecapping, void fraction, acoustic noise emitted by bubbles, etc., will be of little assistance if we are seeking to understand the causes of breaking.

In this paper, as in Babanin *et al.* (2007*b*), we suggest that the incipient breaker is defined dynamically as a wave which has already reached its limiting-stability state, but has not started the irreversible breaking process. That is, breaking onset is the ultimate point at which the wave dynamics caused by initial instabilities is still valid. The state of breaking onset is instantaneous unlike breaking-in-progress which can be further subdivided into a number of stages with different properties and different dynamics (Liu & Babanin 2004).

3.1. *Laboratory set-up*

The laboratory experiment was conducted in the Air–Sea Interaction Salt-Water Tank (ASIST) at RSMAS, University of Miami (http://peas.rsmas.miami.edu/groups/asist). The tank is a stainless-steel construction with a working section of $15\,\mathrm{m} \times 1\,\mathrm{m} \times 1\,\mathrm{m}$. Its programmable fan is capable of generating centreline wind speeds in the range of 0–$30\,\mathrm{m\,s^{-1}}$. Immediately downstream of the fan, extensive flow straightening devices are installed to condition the air flow and introduce appropriately scaled turbulence. Values of wind speed U used in this paper will be those extrapolated to $10\,\mathrm{m}$ height.

ASIST includes a fully programmable piston wavemaker able to produce both monochromatic waves and waves with a predefined spectral form. A set of dedicated measurements showed that amplitude of the first harmonics is of the order of $1\,\%$ of the amplitude of sinusoidal waves generated by the piston in the range of steepness ak between 0.25 and 0.3. These waves are dissipated at the opposite end of the facility by a minimum-reflection beach. The ASIST beach design has been a subject of a special research project. A gently sloping ($10°$) grid of 2.5 cm diameter acrylic rods is used. A perforated acrylic plate is placed beneath the rods to split wave orbital velocities into multiple turbulent jets to increase viscous dissipation. The energy of the reflected component is approximately $5\,\%$ of the incident energy depending on the initial wavelength.
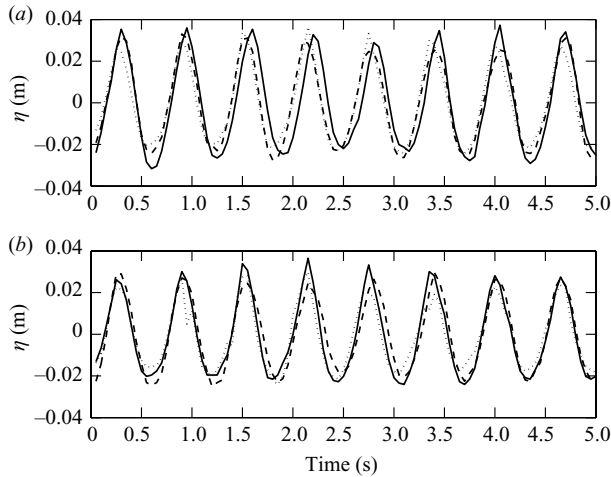
FIGURE 5. Time series of surface elevations η measured at the first wave probe. (*a*) Waves of $U/c = 0$ and $IMF = 1.6$ Hz for different IMS: 0.31 (solid line), 0.25 (dashed line), 0.23 (dotted line). (*b*) Waves of $IMS = 0.23$ and $IMF = 1.6$ Hz under different wind forcing: $U/c = 0$ (solid line), $U/c = 1.4$ (dashed line), $U/c = 11$ (dotted line). The waves propagate from right to left.

In ASIST, sloshing motion becomes increasingly important at wave frequencies exceeding 2.2 Hz. For frequencies below 2 Hz, the waves remain two-dimensional with phase fronts perpendicular to propagation direction. Therefore, our laboratory experiments with two-dimensional waves were limited to frequencies below 2 Hz.

In the present experiment, monochromatic deep-water two-dimensional wavetrains were generated by the wave paddle. The water depth was held at 0.4 m, providing deep-water conditions for the wave frequencies involved. With a tank length of 13.24 m, surface elevations were recorded at 4.55, 10.53, 11.59 and 12.56 m from the paddle. For each record, IMS was varied in such a way that the waves would consistently break just after one of the wave probes. In this way, the dimensional distance to breaking, wavetrain properties immediately prior to breaking and detailed properties of the incipient breaker could be measured. Note that this breaker is a result of nonlinear wave evolution, and its physics is different to, for example, breaking due to coalescing wave packets.

In figures 5 and 6, time series of surface elevations η at the first and the second wave probes are shown. All the waves in these time series are generated with the same initial monochromatic frequency $IMF = 1.6$ Hz, but with different initial steepness IMS and wind forcing U/c, as indicated.

Figure 5(*a*) corresponds to zero wind forcing. Since the initial steepness of $IMS = 0.31$ (solid line), 0.25 (dashed line) and 0.23 (dotted line) is quite high, modulation is already visible developing at the first probe, 4.55 m from the wavemaker. At this stage, the modulation is still quite weak, and differences other than those due to the initial wave height are hardly distinguishable.

In figure 5(*b*), waves of $IMS = 0.23$ are plotted with no wind forcing (solid line, for cross-reference with figure 5*a*), $U/c = 1.4$ (dashed line) and a very strong wind of $U/c = 11$ (dotted line). The effect of the wind on the profile of the mechanically generated waves is not noticeable at this first probe, except for the extreme forcing case, where wind-generated ripples are clearly visible in the time series.
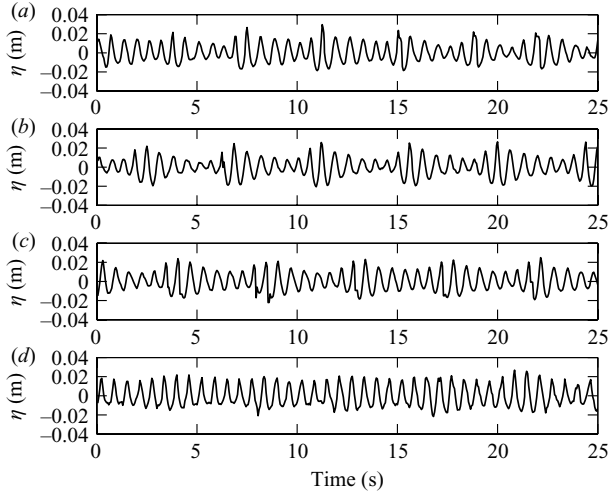
FIGURE 6. Time series of surface elevations η measured at the second wave probe, $IMF = 1.6\,\text{Hz}$. (*a*) $IMS = 0.31$, $U/c = 0$; (*b*) $IMS = 0.25$, $U/c = 0$; (*c*) $IMS = 0.23$, $U/c = 0$; (*d*) $IMS = 0.23$, $U/c = 11$. The waves propagate from right to left.

The wave profiles look very different at the second probe, 10.53 m from the paddle, some 10 wavelengths downstream (figure 6). In all the cases, breaking still has not occurred. Waves in figure 6(*a–c*) evolve without wind forcing, and in the bottom subplot waves are shown strongly forced ($U/c = 11$).

Figure 6(*a*) shows initially very steep waves of $IMS = 0.31$. By the time they reach the second probe, they have developed into very strongly modulated groups of six waves. Less initially steep waves ($IMS = 0.25$, figure 6*b*) evolve into groups of some seven waves. Even less steep waves ($IMS = 0.23$, figure 6*c*) exhibit groups of approximately 7.5 waves (15 waves in two modulations). Note that no initial modulation was introduced. This observation is consistent with the discussion in §1, i.e. if M_I for the system does not change, a larger initial steepness should lead to fewer waves in the modulation.

The effect that the wind forcing has on BF modulation is demonstrated in figure 6(*d*). Here, we define the modulation depth R to be

$$R = \frac{H_h}{H_l}, \tag{3.1}$$

where H_h and H_l are the heights of the highest and lowest waves in the group. In figures 6(*c*) and 6(*d*) waves of $IMS = 0.23$ are shown with and without wind, respectively. The influence of wind is revealed in the reduction in R from 2.1 without wind to 1.3 with a wind of $U/c = 11$. As pointed our by our reviewer, it is the crests' change that appears the main reason for the sharp decrease in R.

It was observed that this change also led to a very significant reduction in the breaking severity (§3.4). The severity (energy loss in a breaking event) is a very important breaking property as, along with the frequency of breaking occurrence (breaking rate), it defines the energy dissipation in a wave field.

3.2. *Measurements of the evolution of nonlinear waves to breaking*

Nonlinear evolution of two-dimensional laboratory waves to breaking will now be investigated in a fashion similar to the numerical study of §2. The nonlinear
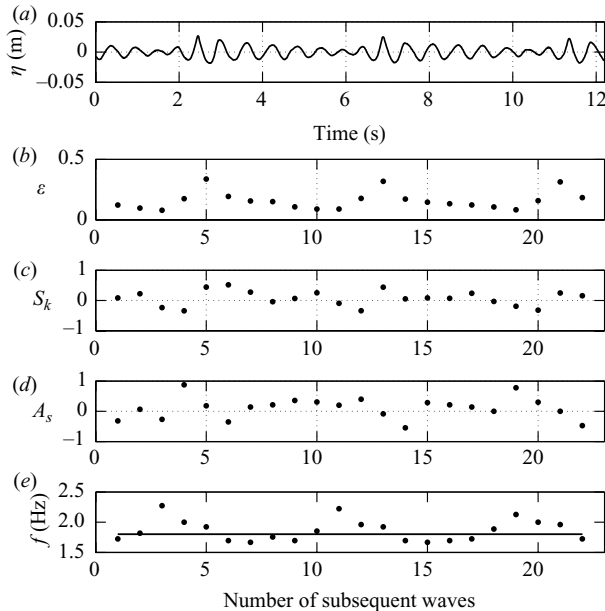
FIGURE 7. Segment of a time series with $IMF = 1.8$ Hz, $IMS = 0.30$, $U/c = 0$. (*a*) Surface elevation η, (*b*) rear-face steepness ϵ, (*c*) skewness S_k (rear-trough depth is used). (*d*) asymmetry A_s, (*e*) frequency, $IMF = 1.8$ Hz is shown by the solid line. The waves propagate from right to left.

characteristics of interest (i.e. individual wave steepness, skewness and asymmetry) will be obtained by means of zero-crossing selection and analysis of individual waves. In addition to these three characteristics, we will scrutinize the behaviour of the period (frequency) of individual nonlinear waves. This feature was not identified in the dimensionless numerical simulations, but in the laboratory it appears to be quite variable, even in the train of waves of initially uniform frequency. The effect of such local frequency variation is significant for the breaking onset study since, when wave height growth is accompanied by a synchronous reduction of wave period, this has a combined impact on the local wave steepness.

It should be noted that there is a conceptual change in the frame of reference compared to the numerical model results. In the case of the model, a single wave was followed as it approached the point of breaking. Here, observations are made at a single point as a succession of waves passes.

Figure 7 shows a wave record with $IMF = 1.8$ Hz, $IMS = 0.30$ and no wind forcing, measured at the second probe. In figure 7(*a*), the measured water surface elevation η is plotted as a function of time in seconds, and in all the other subplots the dots correspond to the successive waves selected by zero-crossing means. The highest waves in each modulation are incipient breakers as IMS was chosen such that the point of breaking was located immediately after the probe at a distance of 10.73 ± 0.1 m from the wavemaker. The apparent consistency of the shape of these near breakers allows an investigation of characteristic geometric properties of the breaking onset (see §3.3). H is always defined in terms of the rear height, and thus the local steepness and skewness are the rear-face steepness and skewness.

Steepness, skewness, asymmetry and frequency of the individual waves are shown in figure 7(*b–e*). The major features seen in the numerical model are confirmed by
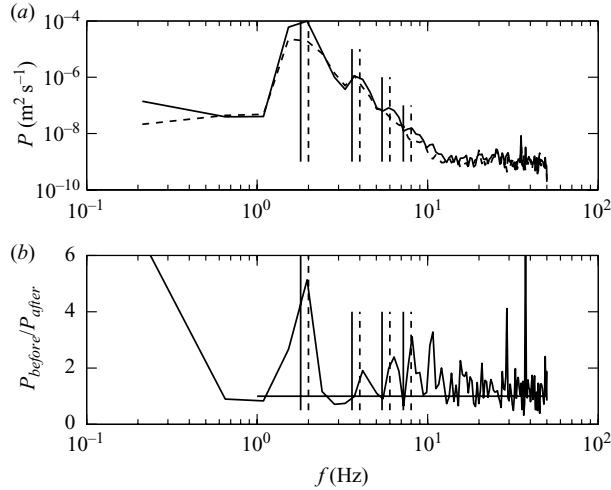
FIGURE 8. (*a*) Spectra *P* of the time series of *IMF* = 1.8 Hz, *IMS* = 0.30, *U*/*c* = 0. Solid line corresponds to the pre-breaking spectrum measured at the second probe (see time series in figures 7). Dashed line is post-breaking spectrum measured at the third probe (time series in figure 9). Multiples of *IMF* are shown with solid vertical lines. Multiples of the incipient breaker 2 Hz frequency are shown with dashed vertical lines. (*b*) Ratio of the pre-breaking and post-breaking spectra. Solid horizontal line signifies ratio of 1, vertical lines have the same meaning as in (*a*).

the laboratory data. In particular, at the point of breaking, skewness is positive and maximal (i.e. wave is peaked up) whilst asymmetry is small (i.e. wave is not tilted forwards) and keeps decreasing.

It is worth mentioning that oscillations of the skewness and asymmetry obtained in our two-dimensional simulations and experiments are also observed in directional wave fields. In Agnon *et al.* (2005), a methodology was developed to describe fine-scale inhomogeneity of wave-field skewness and asymmetry. Continuous time series of skewness were obtained as a running average of the third moment of surface elevation, and asymmetry as a running average of the third moment of the Hilbert transform of the surface elevation. It was found that in field conditions wave skewness and asymmetry oscillate at a scale of a few wave periods.

A feature which was not determined from the dimensionless numerical model is that there is also a modulation of the frequency of individual waves (figure 7*e*). This modulation takes place at the same scale as oscillations of the other nonlinear characteristics. At the point of breaking the frequency increases rapidly. The combined sudden increase in the wave height and contraction of the wave period prior to breaking is a significant feature of the breaking onset. If, as suggested in §2, loss of water-surface stability rather than anything else defines the breaking, then this feature certainly contributes to reaching the critical local steepness. Once detected, for example by wavelet techniques, it may signify the imminent onset of breaking.

This change of frequency prior to breaking is further illustrated in figure 8(*a*) where the spectrum of the time series of figure 7 is plotted. If the wave of *IMF* = 1.8 Hz simply evolved into a steep Stokes wave, a 1.8 Hz peak of the spectrum would bring about first, second and third harmonics indicated by the vertical solid lines. In figure 8(*a*), however, the harmonics, as well as the peak itself are now
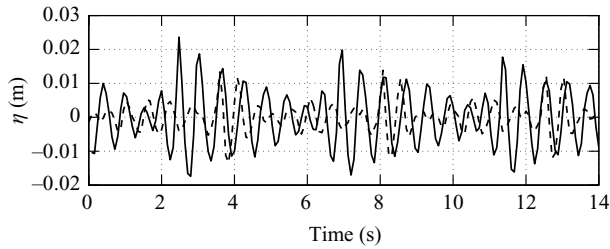
FIGURE 9. The influence of breaking on the time series. A segment of the surface elevation time series with $IMF = 1.8$ Hz, $IMS = 0.30$, $U/c = 0$. Solid line: surface elevations at the second probe prior to breaking; dashed line: same waves 1.2 s later at the third probe. The waves propagate from right to left.

defined by the incipient breaker. The harmonics are located at double, triple and quadruple frequencies of this breaker whose frequency is about 2 Hz (vertical dashed lines).

Therefore, immediately prior to breaking, a frequency upshift of the spectral energy occurs in the laboratory two-dimensional situation (see also figures 10 and 11). Combined with the sudden growth of the wave height at the imminent breaking, this feature has been previously used to detect the breaking events in directional wave fields (Liu & Babanin 2004). Again, this is indirect, but encouraging corroboration that the present two-dimensional study may have relevance for real three-dimensional waves.

In addition, independent observations report a frequency downshift due to breaking (e.g. Tulin & Waseda 1999; Meza, Zhang & Seymour 2000). Wave series immediately before and after the breaking are compared in figure 9. In figure 9, the solid line shows the waves of $IMF = 1.8$ Hz, $IMS = 0.30$, $U/c = 0$ at the second probe (10.53 m from the wavemaker), as in figure 7, and dashed line – at the third probe (11.59 m from the paddle). Breaking of the three incipient breakers seen at the second probe happened (started and finished) between the two probes. The wave which is seen following the incipient breaker at the second probe also broke between the two probes. This consistent double breaking, with a small-time delay, is again in agreement with field observations (e.g. Donelan, Longuet-Higgins & Turner 1972, who observed up to several consequent waves breaking at the top of wave group). These breaking processes happened in a period of 1.2 s, the time required by the 1.8 Hz waves to travel the distance between the probes. Therefore, the record made at the third probe is time shifted by 1.2 s in an attempt to superimpose what should have been the same waves, if the breaking did not take place.

The individual waves and the group propagate with different speeds. In case of deep-water waves of 1.8 Hz frequency shown in figure 9, and in a close-to-linear scenario, the relative speed of wave propagation within the group is $c_{relative} = 0.44$ m s^{-1} and relative position of a wave over 1.2 s will be shifted by 0.52 m. This is comparable with one wavelength of such waves $\lambda = 0.48$ m. That is, in absence of breaking, each wave would approximately move one position ahead, and height of the highest wave would be significantly reduced without any breaking.

Now that breaking has occurred, the correlation between the two time series is poor. The incipient breaker and wave following it practically disappeared, as well as the entire modulation. The number of waves in the segment is also reduced, i.e. frequency downshifting has occurred.

This frequency downshift is analysed in spectral terms in figure 8(a) where, along with the spectrum of time series at the second probe, the third probe spectrum is also plotted. The downshift from the 2 Hz peak of the incipient breaker is very significant, and is also noticeable with respect to $IMF = 1.8$ Hz which was the peak frequency in the wave field before the point of breaking onset. As indicated above, this feature has been observed before (e.g. Tulin & Waseda 1999), and the downshift occurs on a time scale of tens of wave periods. This is is much faster than the scale of thousands of wave periods for the four-wave resonant nonlinear interactions usually attributed with the downshifting. That is, upshifting the wave energy occurs at the point of breaking onset, but the overall effect of the breaking is downshift.

Apart from the frequency downshift, a significant loss of wave energy is observed between the two spectra shown in figure 8(a). In figure 8(b), the ratio of the pre-breaking spectrum to the post-breaking spectrum is plotted. In the range of relevant frequencies up to 11 Hz, the average ratio is 1.8, which translates into a loss of 45 % of the energy. It is most instructive to analyse where this loss comes from.

In both absolute and relative terms, most of the loss came from the peak which was reduced by a factor of 5. With the exception of the second harmonic (shifted to 3.6 Hz), the other harmonics have almost completely disappeared. For frequencies above the spectral peak, the average ratio is approximately 1.7.

This result contradicts observations by Meza *et al.* (2000) who studied the dissipation of energy of laboratory two-dimensional waves with a narrow spectrum. They found that the energy is lost almost entirely from the higher frequencies whereas the spectral peak remained unchanged after breaking. In Meza *et al.* (2000), as in many other laboratory investigations, breaking was simulated by means of coalescing wave packets, i.e. superposition formed a high wave which broke. The limiting steepness of such waves $ak = 0.44$ (Brown & Jensen 2001) is the same as the steepness of the incipient breaker measured in this study (§ 3.3), but the physics of the linear-focusing breaking appears to be quite different to the physics of our experiment.

Under field conditions, Young & Babanin (2006) observed that when the dominant waves break they lose some 30 % of their energy and a similar amount of energy is also lost proportionally across the spectrum, the so-called cumulative effect. By obvious analogy, such observation again suggests the nonlinear evolution mechanism, rather than wave superposition, as a likely cause of wave breaking in the field. The modulational instability may have limitations in directional fields (see discussion in § 4), and it is clear that at least some part of the cumulative effect in the field spectral environment is due to induced breaking (Manasseh *et al.* 2006) and residual turbulent viscosity (Babanin & Young 2005), i.e. reasons other than removal of bound energy observed in figure 8. It is obvious, however, that the modulational instability mechanism is more consistent with field results than the linear-superposition breaking, which does not provide a satisfactory explanation of the observed field features.

3.3. *Measurements of the breaking onset*

While the properties of waves breaking due to focusing coalescing packets have been previously described in great detail (e.g. Rapp & Melville 1990), physical characteristics of breaking resulted from the nonlinear wave evolution have rarely been measured. As the location of the breaker can be controlled by varying the IMS at the wavemaker, the waves were made to break immediately after a wave probe and thus the properties of incipient breakers could be directly estimated.

Quantitative characteristics of these waves are analysed in figures 10 and 11. Figure 10 shows a comprehensive set of statistics of the properties of the 20 highest
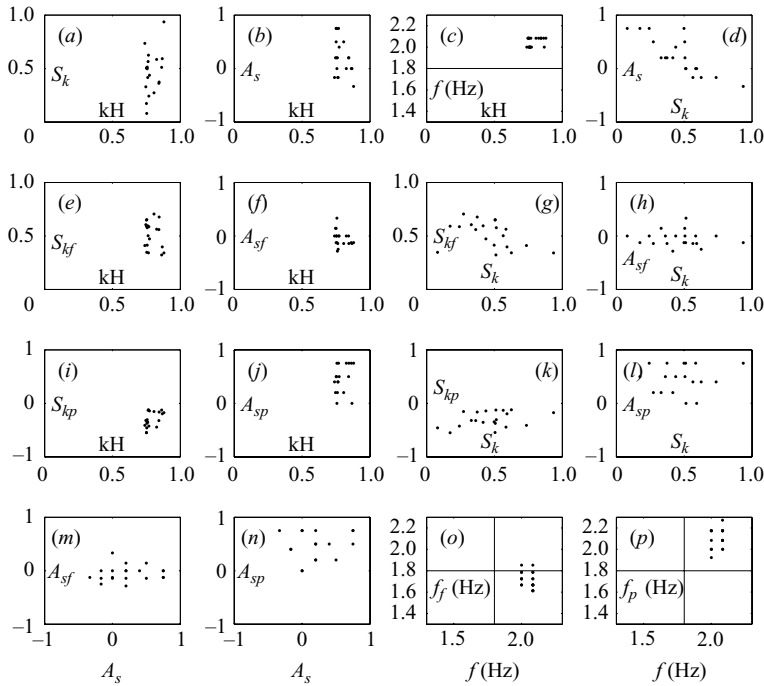
FIGURE 10. Laboratory statistics for the incipient breaker (20 steepest breakers). $IMF = 1.8$ Hz, $IMS = 0.30$, $U/c = 0$. S_{kf} and S_{kp} correspond to the skewness of the following wave and preceding wave respectively, A_{sf} and A_{sp} to the asymmetry of the following wave and preceding wave respectively, f_f and f_p to the frequency of the following wave and preceding wave respectively. (*a*) Skewness versus steepness; (*b*) asymmetry versus steepness; (*c*) frequency (inverse period) versus steepness, $IMF = 1.8$ Hz is shown with solid line; (*d*) asymmetry versus skewness; (*e*) S_{kf} versus steepness of the breaker; (*f*) A_{sf} versus steepness of the breaker; (*g*) S_{kf} versus skewness of the breaker; (*h*) A_{sf} versus skewness of the breaker; (*i*) S_{kp} versus steepness of the breaker; (*j*) A_{sp} versus steepness of the breaker; (*k*) S_{kp} versus skewness of the breaker; (*l*) A_{sp} versus skewness of the breaker; (*m*) A_{sf} versus asymmetry of the breaker; (*n*) A_{sp} versus asymmetry of the breaker; (*o*) f_f versus frequency of the breaker, $IMF = 1.8$ Hz is shown with solid lines; (*p*) f_p versus frequency of the breaker, $IMF = 1.8$ Hz is shown with solid lines.
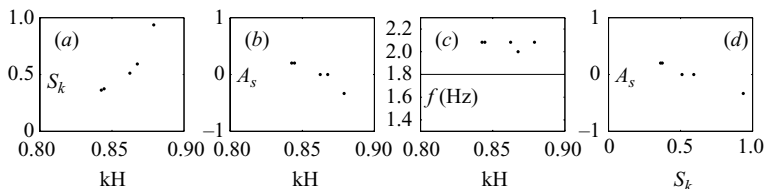

FIGURE 11. As the top four subplots in figure 10, for five steepest breakers.

incipient breakers and their relationship with the preceding and following wave. Figure 10(*a*) is a plot of skewness versus steepness. Values of limiting local steepness, the property which was revealed by the model as the likely indicator of breaking, is in the range of $2\epsilon \approx 0.8$. For a real wave, even if two-dimensional, such steepness is extremely high. Noting that near the crest the wave is even steeper, it is not surprising that the wave is about to break.

The skewness of the 20 highest waves in figure 10(*a*) scatter from almost 0 to almost 1. As indicated in the simulations in §2, we would expect the skewness to also have a limiting value. Clearly, however, such a limit is not a robust breaking characteristic. Asymmetry is also scattered, from $A_s = -0.33$ to $A_s = 0.75$ (figure 10*b*).

A robust property of the breaking, in figure 10(*c*), is the wave frequency. The scatter of this property is small, with all the values falling into a range from $f = 2$ to 2.08 Hz (from 1.11 to 1.16 *IMF*). Thus, the wave clearly reduces in length prior to collapse. We should mention that the measured steepness $\epsilon = kH/2$ is the physical rear-face steepness, and therefore the effect of period contraction has already been accounted for.

In figure 10(*e–h*), the skewness of the wave following the incipient breaker (figure 10*e*) and its asymmetry (figure 10*f*) are much less scattered than the skewness and asymmetry of the breaker itself: $S_{kf} = 0.32$ to 0.70, $A_{sf} = -0.29$ to 0.33. We have already discussed the double breaking in §3.2, which means that this following wave will break soon after the incipient breaker. Thus, its physical shape is not random and should exhibit some characteristic properties leading to breaking. The skewness and asymmetry of the following wave, however, do not correlate with the skewness and asymmetry of the breaker (figures 10*g*, 10*h* and 10*m*).

In figure 10(*i–l*), the skewness of wave preceding the breaker is even less scattered: $S_{kp} = -0.55$ to $+0.12$ (figure 10*i*). Remarkably, it is essentially negative, i.e. rear trough of the preceding wave is always deeper than its crest. The asymmetry $A_{sp} = 0–1.33$ is never negative (a couple of large $A_{sp} = 1.33$ values are off scale in figure 10*j* and not shown), that is this wave is tilted backwards. There is no correlation of skewness and asymmetry of this preceding wave with those of the near-breaker (figures 10*k*, 10*l* and 10*n*). The fact that the three waves, surrounding the breaking event, obviously exhibit some quasi-universal form, but that variations of their shape are not correlated with each other, means that these shape distortions are random. Therefore, it is not the mean characteristics of the observed shapes, but rather their limiting values which should produce asymptotic universal form parameters. These will be investigated for the highest breakers in figure 11.

Figure 10(*o*, *p*) shows the local frequency of the following f_f and preceding f_p waves versus the frequency of the breaker f_b. $IMF = 1.8$ Hz is shown with two solid lines. Although f_f and f_p are more scattered than f_b, the correlation is present. In figure 10(*p*), all the data points are in the second quadrant and thus the preceding wave is decreasing in length along with the incipient breaker. In figure 10(*o*), the points are on average in the fourth quadrant. Therefore, while the incipient breaker is decreasing in length, the following wave is actually longer than its initial value defined by $IMF = 0.18$ Hz. Since we know that double breaking will occur, this following wave should now be rapidly shrinking. Thus, some very active physics must be involved in the short time scale evolution of this set of very nonlinear waves.

Figure 11 shows asymptotic, rather than statistical properties of the incipient breaker. In figure 11, the characteristics of the five steepest waves are plotted. As discussed above, transition to breaking happens very rapidly, and breaking onset and its location may be somewhat modulated due to, for example, uneven number of waves in the nonlinear oscillations. Thus, we would expect that it is the highest waves measured that would be closest to the ultimate limiting characteristics of the incipient breaker.

For the steepest five waves shown in figure 11, the asymptotic dependence of skewness on steepness is very clear (figure 11*a*). Note that the bottom scale of figure 11 t is different to that of figure 10. For the 20 steepest incipient breakers,
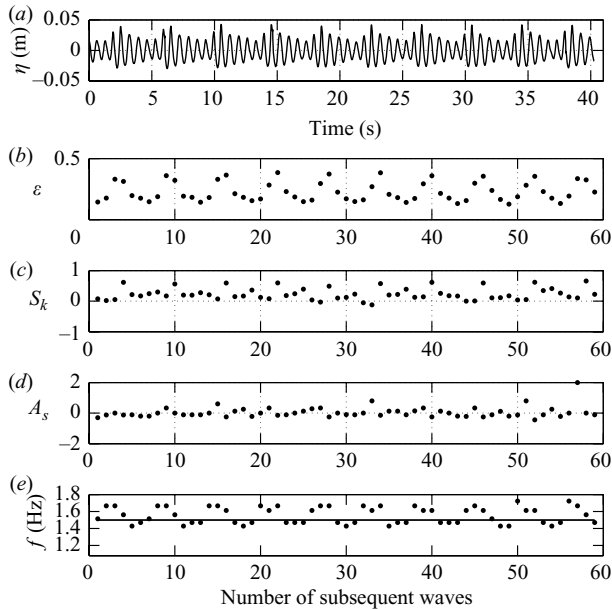
FIGURE 12. As in figure 7, with wind forcing. A segment of the time series with $IMF = 1.5\,\text{Hz}$, $IMS = 0.30$, $U/c = 3.9$. (*a*) Surface elevation η; (*b*) rear-face steepness ϵ; (*c*) skewness S_k (rear-trough depth is used); (*d*) asymmetry A_s; (*e*) frequency (inverse period), $IMF = 1.5\,\text{Hz}$ is shown with solid line. The waves propagate from right to left.

skewness was broadly scattered, now that onset is close, it asymptotes to a value of 1, i.e. crest of the wave is twice as high as its trough (2.16).

The steepness appears to approach an asymptotic limit of $\epsilon = kH/2 \approx 0.44$ which apparently represents an absolute steepness limit (Babanin *et al.* 2007*b*). We should point out that this limit is remarkably close to the theoretical steady limiting steepness of $ak = 0.443$, i.e. the Stokes limit $H/\lambda = 1/7$ where $\lambda = 2\pi/k$ is the wavelength. Such an observation is very important because it signifies that the waves break once they achieve this well-established state, beyond which the water surface cannot retain its stability. Thus the limiting steepness, rather than anything else, will trigger the breaking. We can postulate that the other geometric, kinematic and dynamic criteria of breaking, explored in the literature, are indicative of a wave approaching this state, but are not a reason or a cause for the breaking. As this limit is approached, the asymmetry starts to decrease and becomes negative (figures 11*b* and 11*d*), i.e. the wave starts tilting forwards.

3.4. *Laboratory investigation of the influence of wind forcing*

Following the approach of §2, we now investigate the influence of wind on the nonlinear wave evolution and breaking onset. Figure 12 is similar to figure 7, but moderately strong wind forcing of $U/c = 3.9$ is now applied to the mechanically generated waves. Note that $IMF = 1.5\,\text{Hz}$ is different from $IMF = 1.8\,\text{Hz}$ in figure 7. This is done in order to have incipient breakers, as before, at the probe 2 where data is recorded.

In figure 7, $R = 4$ whereas in figure 12, $R = 2.9$, i.e. the difference in the modulation depth is 1.4 times. Thus, we observe the expected feature of smearing of the modulation by the wind. This smearing is reflected in all the other nonlinear properties shown in the figure. The steepness (figure 12*b*), skewness (figure 12*c*) and asymmetry (*d*) are
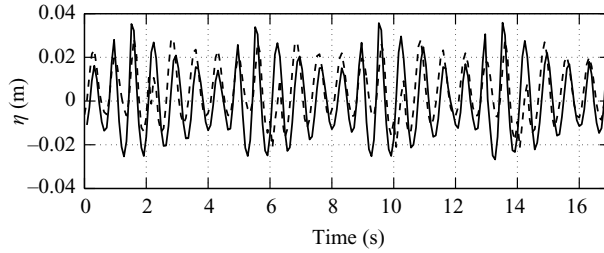
FIGURE 13. As in figure 9, with wind forcing. A segment of the time series with $IMF = 1.5\,\mathrm{Hz}$, $IMS = 0.30$, $U/c = 3.9$. Solid line: surface elevations at the second probe prior to breaking; dashed line: same waves 1.04 s later at the third probe. The waves propagate from right to left.

intentionally plotted at the same scale as those in figure 7 even though their range of oscillations is now noticeably reduced. Because of the *IMF* change, the scale of the frequency plot (*e*) could not be left the same, but scale limits were kept proportional to those in figure 7. Reduction of the local frequency oscillations, moderated by the wind, is also apparent.

Influence of the smearing on the wave breaking is demonstrated in figure 13. This figure is analogous to figure 9 except the wind forcing is imposed and $IMF = 1.5\,\mathrm{Hz}$ is different. The wave time series are compared immediately before and after breaking. The solid line shows the waves of $IMF = 1.5\,\mathrm{Hz}$, $IMS = 0.30$, $U/c = 3.9$ at the second probe (10.53 m from the maker) and the dashed line at the third probe (11.59 m from the paddle). Breaking of the four incipient breakers seen at the second probe occurred (started and finished) between the two probes. The breaking was very gentle when visually observed. The wave following this gentle incipient breaker now does not break, i.e. the wind cancelled the double-breaking effect. With $IMF = 1.5\,\mathrm{Hz}$, the time necessary to travel the distance between the two probes is estimates as 1.04 s and therefore the record made on the third probe is shifted back by 1.04 s in order to superpose what should be the same waves if the breaking did not take place.

Since gentle breaking did occur, matching the two series is not exact. In figure 9, the incipient breaker and the wave following it practically disappeared, as well as the entire modulation. Here they are all present and each wave in the modulation can be tracked at the third probe. In contrast to figure 9, after breaking the number of the waves did not change and no downshifting is visible. As seen in the figure, the breaking resulted in truncation of the crest of the breaker and smoothing of the modulation. It should be pointed out that the individual waves and the group propagate with different speeds which fact also accounts for some differences observed.

In figure 14, analogous to the no-wind figure 10, the statistics of a comprehensive set of properties for the 20 highest incipient breakers and their links to the preceding and following wave are shown. For the 20 waves approaching breaking, the wind influence generally brought more order to their shapes, as the scatter of almost all the properties is reduced and the marginal dependences became clearer. Qualitatively, the wind changed the shape of the preceding wave which is now not skewed negatively on average (figure 14*i*) and increased the steepness of the following wave from $\epsilon = 0.19$ to $\epsilon = 0.27$ on average (not shown).

With regard to the asymptotic shape of the breaker, the wind in figure 15 has a scattering rather than a stabilizing influence. In figure 15, analogous to figure 11, characteristics of the five steepest waves are plotted in the presence of wind.
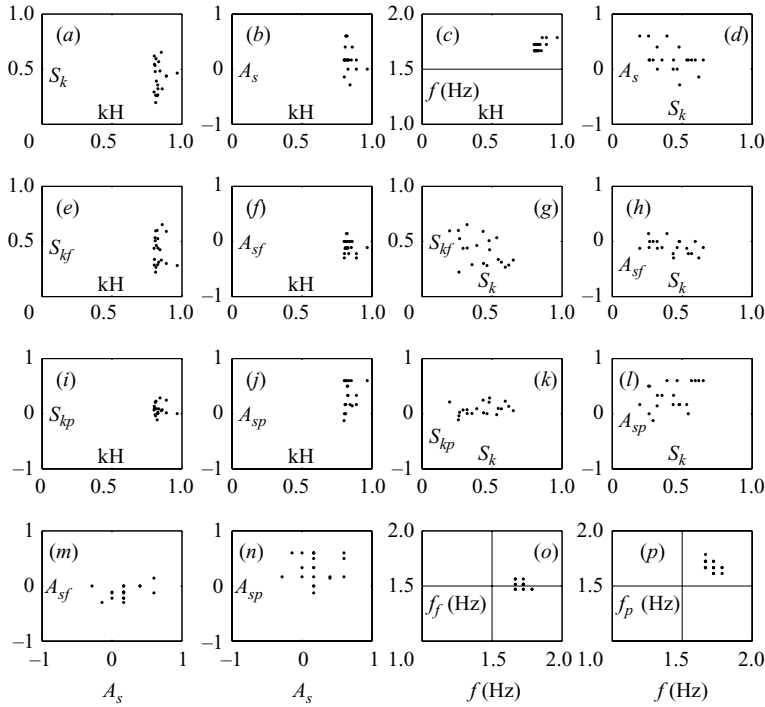
FIGURE 14. As in figure 10, with wind forcing: $IMF = 1.5\,\text{Hz}$, $IMS = 0.30$, $U/c = 3.9$. Laboratory statistics for 20 steepest incipient breakers.
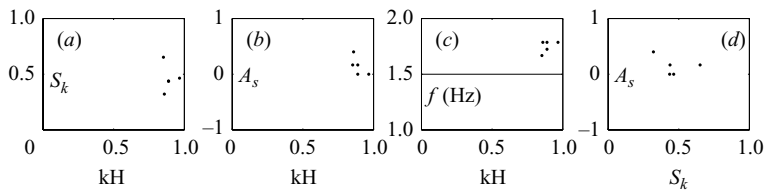

FIGURE 15. As figure 11, with wind forcing: $IMF = 1.5\,\text{Hz}$, $IMS = 0.30$, $U/c = 3.9$. Laboratory statistics for five steepest incipient breakers.

Apparently, at these very last pre-breaking stages, the wind is capable of modifying the wave, which is about to lose its stability, and to somewhat randomize its characteristics. In figure 15(*a*), the limiting skewness is plotted versus limiting steepness. Skewness no longer approaches 1, but steepness extends beyond the $2\epsilon = 0.88$ limit and reaches $2\epsilon = 0.97$. The asymmetry is no longer negative, that is, the breakers do not tilt forwards (figure 15*b*). Frequency remains a robust property and stays in almost the same range of $f_b = 1.11$–$1.19\ IMF$ (figure 15*c*).

Therefore, whilst the breaking is mainly a hydrodynamic process, wind, if present, does influence the incipient breaking. As was noticed in the numerical simulations, this influence is small, but it is noticeable and diverse – from the shape-stabilizing effect when approaching breaking onset to the shape-randomizing effect at the point of breaking.
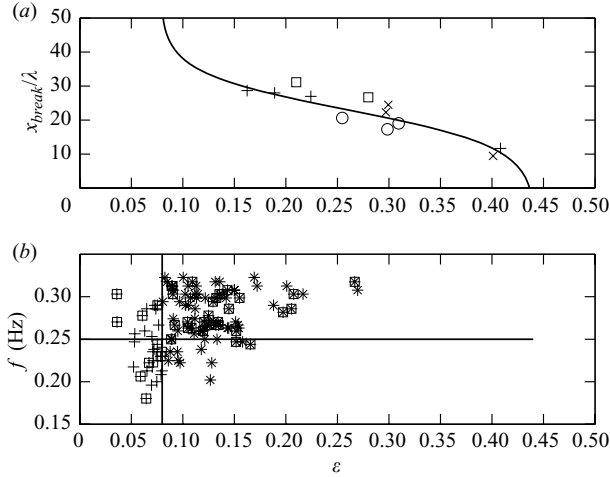
FIGURE 16. (*a*) ASIST laboratory data. Number N of wavelengths to breaking versus *IMS*. No wind forcing. $\circ$: $IMF = 1.6$ Hz; $\times$: $IMF = 1.8$ Hz; $+$: $IMF = 2.0$ Hz. The parameterization (4.1) is shown with solid line. Squares are data points derived from Melville (1982). (*b*) Black Sea. Properties of individual waves in the range of frequencies $f = f_p \pm 0.3 f_p$ of a Black Sea record with $f_p = 0.25$ Hz. Frequency (inverse period) f versus steepness ϵ. $+$: all waves; $*$: those waves with $\epsilon > 0.08$; squared: those waves exhibiting whitecapping. Solid lines show peak frequency $f_p = 0.25$ Hz (horizontal) and the breaking threshold $\epsilon = 0.08$ (vertical).

4. Discussion and conclusions

In the numerical simulations of §2, figure 3 was the main result because it allowed us to predict the distance to breaking in dimensionless terms: number of wavelengths to breaking $N = x_{break}/\lambda$ as a function of wave steepness and wind forcing, where x_{break} is the dimensional distance. Examination of its laboratory analogue was moved to this section as its applicability to field conditions will also be discussed.

The laboratory dependence of the distance-to-breaking on *IMS* was obtained and parameterized in Babanin *et al.* (2007*b*). The relevant figure 5(*a*) of Babanin *et al.* (2007*b*) is reproduced with modifications as figure 16(*a*) here. Number N is plotted versus *IMS* for three different initial frequencies of $IMF = 1.6$ Hz (circles), $IMF = 1.8$ Hz (crosses) and $IMF = 2.0$ Hz (pluses). All the measurements shown are conducted without wind.

In accordance with the numerical simulations, for each wavelength an increase of its initial steepness resulted in the breaking occurring closer to wavemaker. In dimensionless terms, this dependence was parameterized as follows:

$$N = -11 \text{ arc tanh}(5.5(\epsilon - 0.26)) + 23 \text{ for } 0.08 \leqslant \epsilon \leqslant 0.44. \qquad (4.1)$$

Consistent, with the model results, the formula imposes two threshold values of *IMS*. For $\epsilon > 0.44$, the wave breaks immediately (compared to $\epsilon = 0.3$ for the model) and if $\epsilon < 0.08$ the wave, in the absence of wind forcing, will never break (compared to $\epsilon = 0.1$ for the model). In the figure, two points (squares) are also shown which were derived from figures 1 and 2 of Melville (1982) for comparison.

Comprehensive wind-forcing picture similar to the numerical result in figure 3 could not be obtained in ASIST where available range of distances and wavelengths was limited by the tank dimensions. Besides, as pointed out by our reviewer, presence of a sustained wind in the tank may cause a significant shear layer and vorticity field
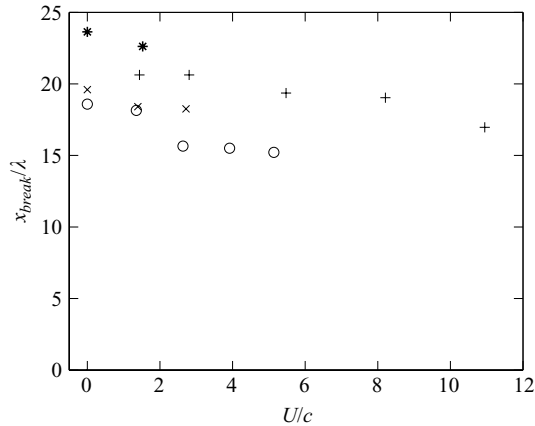
FIGURE 17. Number N of wavelengths to the breaking versus wind forcing U/c. o:
$IMF = 1.5\,\mathrm{Hz}$; x: $IMF = 1.55\,\mathrm{Hz}$; +: $IMF = 1.6\,\mathrm{Hz}$; *: $IMF = 1.7\,\mathrm{Hz}$.

in the water. The latter can lead to steeper steady free surfaces and thus make direct quantitative comparisons problematic. Qualitatively, however, the laboratory results are in full accord with numerical simulations. In figure 17, number N is plotted versus wind-forcing parameter U/c for four different IMFs: $IMF = 1.5\,\mathrm{Hz}$ (circles), $IMF = 1.55\,\mathrm{Hz}$ (crosses), $IMF = 1.6\,\mathrm{Hz}$ (pluses) and $IMF = 1.7\,\mathrm{Hz}$ (asterisks). At each IMF, initial steepness IMS was kept constant, and therefore the apparent trend of reduction of distance-to-breaking is due to wind only.

We now discuss the possibility of applying our results to waves in the field. A number of features of nonlinear wave behaviour leading to the breaking, which were revealed both in our two-dimensional simulations/measurements and in known field observations have been mentioned above. These are the double breaking found in our laboratory experiments and observed in the field by Donelan *et al.* (1972), the upshifting of spectral energy (figure 8) observed in Liu & Babanin (2004), oscillations of the skewness/asymmetry (figures 2 and 7) in Agnon *et al.* (2005) and cumulative effect (figure 8) in Young & Babanin (2006). Gemmrich & Farmer (2004) analysed velocity field under the passing breaker and found upshifting of wave energy followed by downshifting (figure 12 in Gemmrich & Farmer 2004), which is qualitatively similar to the upshifting–downshifting observed in this paper (figures 8 and 9). Similarly, conclusion of Melville & Matusov (2002) about breaking waves propagating at some 80 % of the characteristic linear phase speed can be interpreted as an indirect support of the pre-breaking wave shrinkage. The fact that doubling the wind input brings about wave breaking four times as fast (§ 2.2, figure 2) is consistent with field experiments on wind input (Donelan *et al.* 2006). Although all these indicators of the modulational instability behaviour are indirect, they are many and diverse.

What is against direct extrapolation of outcomes of the present paper into field conditions is known experimental and theoretical results on limitations which BF mechanism has in broadband, and particularly in three-dimensional fields (e.g. Brown & Jensen 2001; Onorato *et al.* 2002, 2009; Waseda, Kinoshita & Tamura 2009). We concluded that modulational instability is the driving force behind nonlinear evolution of our waves to breaking, and since our study was initially monochromatic and two-dimensional, and field waves are spectral and directional, this issue has to be addressed before applying our results to such waves.

Brown & Jensen (2001) studied the focusing of unidirectional waves and found that BF instability is impaired in focusing (i.e. spectral) wavetrains. Such study needs to be extended into spectra typical of field waves and examined further. There is a reasonable expectation, however, that the modulational mechanism may work for reasonably steep waves with a narrow spectrum (e.g. Waseda *et al.* 2009). For unidirectional spectral waves, Alber (1978) derived a requirement which can be expressed as

$$M_I > 1, \tag{4.2}$$

and this condition can be satisfied for spectra of young wind waves (e.g. Onorato *et al.* 2001).

There is no analogue of M_I and condition (4.2) available for three-dimensional characteristics of the modulational instability mechanism. In Onorato *et al.* (2002), directional effects were investigated and quantitative criterion β was obtained in terms of width of directional spectrum $D(\theta)$ where θ is angle in radians:

$$D(\theta) = \cos^2\left(\frac{\pi}{2\beta}\theta\right), \tag{4.3}$$

i.e. if the directional width is greater than $\beta = 15$, the modulational instabiltiy appears to be suppressed. There was a typing error in Onorato *et al.* (2002), and value of β has to be actually multiplied by $\pi/180$, that is the criterion is $\beta \approx 0.26$ (Onorato, personal communication 2007). Since the Onorato *et al.* (2002) model is weakly nonlinear rather than fully nonlinear, the criterion should only be regarded as an approximation, but we will use it as a reference point here.

To compare width of the (4.3) spectrum with observations, integral value A was estimated:

$$A^{-1} = \int_{-\beta}^{\beta} D(\theta)\,d\theta, \tag{4.4}$$

which was used in the field study of Babanin & Soloviev (1987, 1998*a*) to measure directional distributions (the higher is A, the narrower is the spectrum). For $\beta = 0.26$, $A = 3.8$ which is well above the experimentally observed values. It should be mentioned that this theoretical value is in excellent agreement with the laboratory experiment of Waseda *et al.* (2009) who concluded that the critical directional spread is $A \approx 4$.

Modulational instability, however, may still be found applicable, at least for the dominant waves if they are steep enough. It is not unreasonable to expect a directional condition analogous to (4.2) being relevant. Parameter A (4.4) can be used for this purpose as it has the proper physical meaning of the inverse relative width of the directional spectrum whose peak is normalized to be 1.

At the spectral peak, a relative steepness (as the wave spectrum develops) is defined by $\sqrt{\gamma}$ where γ is the peak enhancement of the JONSWAP spectrum. That is, for the peak, we can define a directional analogue of M_I as

$$M_{Id} = A\sqrt{\gamma}. \tag{4.5}$$

Now, it is informative to look at how this Index evolves over the wave development. From (19) of Babanin & Soloviev (1998*a*), at the spectral peak

$$A = 1.12\left(\frac{U_{10}}{c_p}\right)^{-0.50} + (2\pi)^{-1}, \tag{4.6}$$

and from (44) of Babanin & Soloviev (1998*b*):

$$\gamma = \frac{7.6}{2\pi} \frac{U_{10}}{c_p}, \tag{4.7}$$

that is,

$$\sqrt{\gamma} = 1.10 \Big(\frac{U_{10}}{c_p} \Big)^{0.50}. \tag{4.8}$$

Therefore,

$$M_{Id} = 1.23 + \frac{1.1}{2\pi} \Big(\frac{U_{10}}{c_p} \Big)^{0.50} \tag{4.9}$$

is a weak function of the wind forcing, and its value at the spectral peak varies from 1.40 to 1.79 for U_{10}/c_p in the range from 0.89 to 10 where $U_{10}/c_p = 0.89$ signifies full development (Pierson–Moscowitz limit).

Now, if the M_{Id} assumption is valid and the critical value for this Index is in the range of $M_{Id} = 1.4$–1.8, the 'focusing' effect of directionality can be overcome by a stronger nonlinearity if waves grow steeper. It is worth noting here that the directional spectra broaden towards frequencies above the peak (e.g. Babanin & Soloviev 1998*a*). This means that, even if applicable at the peak, the directional modulational instability may not be working at higher frequencies and some other causes of breaking and dissipation will have to be found in that spectral band. In this regard, two-phase behaviour of the breaking has indeed been observed in field experiments of Babanin & Young (2005); Manasseh *et al.* (2006), i.e. the direct dependence of breaking on spectral density at the peak and an induced breaking/dissipation at higher frequencies.

In any case, the issue of modulational instability in real spectral directional fields cannot be solved now, but with caution we will try to apply our results to the field data. Another problem, of the technical kind, still prevents direct comparisons of breaking rates obtained by means of (4.1) and field observations. Relationship (4.1) predicts the probability of incipient breaking, whereas in the field it is impossible to directly measure whether a wave is an incipient breaker or not. At best, we can detect quantities which result from the breaking process, that is we count waves already breaking. Common measures of this type include the acoustic signature of breaking waves, void fraction or surface whitecap coverage. However, a breaking wave emits sound and forms whitecaps over a substantial part of its period whereas the incipient breaking is an instantaneous state, and therefore the probability of encountering such sound or whitecaps is significantly higher than the probability of breaking onset (Liu & Babanin 2004).

Qualitative comparisons of the laboratory and field breaking-probability dependences were done in Babanin *et al.* (2007*b*) and featured well. Here, in figure 16(*b*) we plot frequency (inverse period) of individual dominant waves (from frequency range of $f = f_p \pm 0.3 f_p$) versus steepness of these individual waves. This is done for a Black Sea record with $f_p = 0.25$ Hz used by Babanin *et al.* (2001) to obtain field breaking rates in the same frequency band. If there was no shrinking of the wavelength prior to breaking, as described in this paper, at each steepness the distribution of the frequencies around $f_p = 0.25$ Hz would be approximately even. It is so for waves of $\epsilon < \approx 0.12$. For steeper waves, and some of these detected deep-water wind-generated three-dimensional waves have an enormous by field standards steepness up to $\epsilon = 0.27$, the distribution is clearly biased towards higher frequencies. Waves with $\epsilon > 0.17$ are all shorter than those of the peak frequency $f_p = 0.25$ Hz, and the higher is the individual steepness, the higher is the individual frequency. Since on average

the highest waves are observed at the peak frequency, and the peak is very sharp, the only plausible explanation for this observation is that these abnormally steep, but rare waves are those in transition towards or just after the incipient breaking. Thus, the very existence of such abnormally high and shrunk waves indicates that the modulational instability mechanism is most likely still active in these field conditions.

It is very informative to see in this plot which waves are detected as breaking by observing whitecaps. Such waves are indicated by squares. Liu & Babanin (2004) classified phases of the wave breaking process into incipient, developing, subsiding and residual stages. At the incipient phase, waves are at their steepest and the surface has already lost its stability, but there are no whitecaps formed. Whitecaps are observed at developing and subsiding stages. The latter phase is characterized by very broken shape of waves and their steepness may be well below the field average. The last, residual stage was introduced formally following Rapp & Melville (1990) as such phase of breaking progress when the whitecap is already left behind, but the turbulent front is still moving downstream.

In figure 16(*b*), vertical solid line identifies the threshold of $\epsilon = 0.08$ below which even two-dimensional waves are not expected to break. Yet, a significant number of them, some with steepness as low as $\epsilon = 0.03$ are detected as whitecapping. This is the subsiding (not breaking) phase, still detected as breaking if relied on whitecap observations. On the other end, out of two waves with $\epsilon \approx 0.27$, one wave does not exhibit whitecaps and another does, that is the first one is on its way up to the limiting steepness and another is on its way down while collapsing. This observations highlights uncertainties and ambiguity of existing definitions of breaking rates.

Finally, we would like to summarize main results, findings and conclusions of the numerical and laboratory investigations of the deep-water breaking in two-dimensional circumstances. Modulational instability mechanism is not the cause of the breaking, as it may or may not lead to the breaking. The breaking will occur if the wave in the course of its nonlinear evolution reaches the limiting steepness, that is the water surface becomes unstable and collapses. Evolution of nonlinear wave properties was mainly investigated in the physical rather than Fourier space. Particular attention was paid to steepness, skewness and asymmetry of individual waves, and to their interplay leading to the breaking onset. Individual wave steepness was found to be the single parameter which determines whether the wave will break immediately, never break or take a finite number of wavelengths to break. Dimensionless distance to the breaking can be parameterized in terms of the wave steepness as the primary parameter. Properties of the incipient breaker were measured in detail.

If the wind forcing is superimposed, it can play multiple roles in affecting the wave-breaking dependences. Wind action is important on longer scales in altering breaking statistics because of enhancing the wave steepness. At moderate winds, doubling the wind speed leads to the limiting steepness and breaking four times as fast. At stronger wind forcing, this effect slows down. Wind capacity to affect the breaking onset at short time scale is marginal unless the wind forcing is very strong.

Detailed laboratory observations revealed a number of additional features of the breaking process. At the breaking onset, wave period decreases (frequency increases) which further instigates the steepness growth towards the limiting state. Wave preceding the breaker is tilted backwards and negatively skewed. Wave, following the breaker is transient. Its steepness, skewness, asymmetry and frequency are all growing, and it breaks soon after the first breaker (double breaking). Features of the shape of the three waves appear to be inter-connected, particularly as the breaking onset is approaching, which fact indicates strong and rapid nonlinear interactions in

the system. At the breaking onset, upshift of the spectral energy takes place. After the breaking, downshifting occurs. Superimposed wind influences the wave modulation and breaking severity. Strong wind makes the breaking more frequent, but smoothens the modulation, cancels the double breaking and reduces the breaking strength. As a result, it affects the total dissipation in an unknown way. This very important issue needs further research.

Nature of breaking process, resulted from the nonlinear evolution and from the coalescing linear waves, is essentially different. While the limiting steepness of $\epsilon = ak = Hk/2 = 0.44$ appears to be the same in both cases, energy loss and distribution of this loss across the spectrum are dissimilar. This conclusion implies significant consequences for wave dissipation studies, i.e. research of the breaking and the dissipation have to be separated. While any process which leads to the critical steepness will cause the wave collapse, their end result in terms of the spectral dissipation will have principle differences. In other words, the breaking is in a way a kinematic effect (i.e. moving water surface becomes unstable, no matter what is a balance of forces other than gravity) whereas the energy dissipation following the breaking is a dynamic process which remembers the history (i.e. depends on the driving forces both before and after the breaking onset).

A significant number of features typical of ocean breaking waves was reproduced in this two-dimensional fully nonlinear study which points out to the modulational instability as a likely mechanism active in the field, at least at the scale of dominant waves. Most important further research, however, is needed into the role of this mechanism in broadband and three-dimensional wave fields, particularly at the shorter wave scales. Since there are theoretical and experimental indications that this mechanism can be suppressed if frequency and directional spectra are broad, nature of wave energy dissipation and breaking can be different in three-dimensional wave fields, particularly at smaller scales characterized by broader angular distributions.

REFERENCES

AGNON, Y., BABANIN, A. V., CHALIKOV, D. & YOUNG, I. R. 2005 Fine scale inhomogeneity of wind–wave energy input, skewness and asymmetry. *Geophys. Res. Lett.* **332**, L12603, doi:10.1029/2005GL022701.

ALBER, I. E. 1978 The effects of randomness on the stability of two-dimensional wavetrains. *Proc. R. Soc. Lond.* **A363**, 525–546.

BABANIN, A. V., BANNER, M. L., YOUNG, I. R. & DONELAN, M. A. 2007a Wave follower measurements of the wind input spectral function. Part 3. Parameterization of the wind input enhancement due to wave breaking. *J. Phys. Oceanogr.* **37**, 2764–2775.

BABANIN, A. V., CHALIKOV, D., YOUNG, I. R. & SAVELYEV, I. 2007b Predicting the breaking onset of surface water waves. *Geophys. Res. Lett.* **34**, L07605, doi:10.1029/2006GL029135.

BABANIN, A. V. & SOLOVIEV, Y. P. 1987 Parametrization of the width of angular-distribution of the wind wave energy at limited fetches. *Izvestiya Akademii Nauk SSSR Fizika Atmosfery: Okeana* **23**, 868–876.

BABANIN, A. V. & SOLOVIEV, Y. P. 1998a Variability of directional spectra of wind-generated waves, studied by means of wave staff arrays. *Mar. Freshwater Res.* **49**, 89–101.

BABANIN, A. V. & SOLOVIEV, Y. P. 1998b Field investigation of transformation of the wind wave frequency spectrum with fetch and the stage of development. *J. Phys. Oceanogr.* **28**, 563–576.

BABANIN, A. V. & YOUNG, I. R. 2005 Two-phase behaviour of the spectral dissipation of wind waves. In *Proceedings of the Ocean Waves Measurements and Analysis, Fifth Intl Symp. WAVES2005, 3–7 July, 2005*, Madrid, Spain (ed B. Edge & J. C. Santas), paper 51, 11p.

BABANIN, A. V., YOUNG, I. R. & BANNER, M. L. 2001 Breaking probabilities for dominant surface waves on water of finite constant depth. *J. Geophys. Res.* **C106**, 11659–11676.

BENJAMIN, T. B. & FEIR, J. E. 1967 The disintegration of wave trains in deep water. Part 1. Theory. *J. Fluid Mech.* **27**, 417–430.

BROWN, M. G. & JENSEN, A. 2001 Experiments in focusing unidirectional water waves. *J. Geophys. Res.* **C106**, 16917–16928.

CAULLIEZ, G. 2002 Self-similarity of near-breaking short gravity wind waves. *Phys. Fluids* **14**, 2917–2920.

CHALIKOV, D. 2005 Statistical properties of nonlinear one-dimensional wave fields. *Nonlinear Process. Geophys.* **12**, 1–19.

CHALIKOV, D. 2007 Simulation of Benjamin–Feir instability and its consequences. *Phys. Fluids* **19**, 016602-15.

CHALIKOV, D. & SHEININ, D. 1998 Direct modelling of one-dimensional nonlinear potential waves. In *Nonlinear Ocean Waves* (ed W. Perrie), Advances in Fluid Mechanics, vol. 17, pp. 207–258. WIT Press.

CHALIKOV, D. & SHEININ, D. 2005 Modelling extreme waves based on equations of potential flow with a free surface. *J. Comput. Phys.* **210**, 247–273.

CRAIG, W. & SULEM, C. 1993 Numerical simulation of gravity waves. *J. Comput. Phys.* **108**, 73–83.

CRAPPER, G. D. 1957 An exact solution for progressive capillary waves of arbitrary amplitude. *J. Fluid Mech.* **96**, 417–445.

DOLD, J. W. 1992 An efficient surface-integral algorithm applied to unsteady gravity waves. *J. Comput. Phys.* **103**, 90–115.

DOLD, J. W. & PEREGRINE, D. H. 1986 Water-wave modulation. In *Proceedings of the Twentieth Intl Conf. on Coastal Engineering*, Taipei, Taiwan, pp. 163–175. ASCE.

DONELAN, M. A., BABANIN, A. V., YOUNG, I. R. & BANNER, M. L. 2006 Wave follower measurements of the wind input spectral function. Part 2. Parameterization of the wind input. *J. Phys. Oceanogr.* **36**, 1672–1688.

DONELAN, M. A., LONGUET-HIGGINS, M. S. & TURNER, J. S. 1972 Whitecaps. *Nature* **36**, 172–1688.

GEMMRICH, J. R. & FARMER, D. M. 2004 Near-surface turbulence in the presence of breaking waves. *J. Phys. Oceanogr.* **34**, 1067–1086.

JANSSEN, P. A. E. M. 2003 Nonlinear four-wave interaction and freak waves. *J. Phys. Oceanogr.* **33**, 863–884.

LIU, P. C. & BABANIN, A. V. 2004 Using wavelet spectrum analysis to resolve breaking events in the wind wave time series. *Ann. Geophys.* **22**, 3335–3345.

LONGUET-HIGGINS, M. S. & COKELET, E. D. 1976 The deformation of steep surface waves on water. I. A numerical method of computation. *Proc. R. Soc. Lond.* **A350**, 1–26.

LONGUET-HIGGINS, M. S. & COKELET, E. D. 1978 The deformation of steep surface waves on water. II. Growth of normal-mode instabilities. *Proc. R. Soc. Lond.* **A364**, 1–28.

LONGUET-HIGGINS, M. S. & DOMMERMUTH, D. G. 1997 Crest instabilities of gravity waves. Part 3. Nonlinear development and breaking. *J. Fluid Mech.* **336**, 33–50.

LONGUET-HIGGINS, M. S. & FOX, M. G. H. 1977 Theory of the almost highest wave: the inner solution. *J. Fluid Mech.* **80**, 721–741.

MANASSEH, R., BABANIN, A. V., FORBES, C., RICKARDS, K., BOBEVSKI, I. & OOI, A. 2006 Passive acoustic determination of wave-breaking events and their severity across the spectrum. *J. Atmos. Ocean. Technol.* **23**, 599–618.

MELVILLE, W. K. 1982 Instability and breaking of deep-water waves. *J. Fluid Mech.* **115**, 165–185.

MELVILLE, W. K. & MATUSOV, P. 2002 Distribution of breaking waves at the ocean surface. *Nature* **417**, 58–63.

MEZA, E., ZHANG, J. & SEYMOUR, R. J. 2000 Free-wave energy dissipation in experimental breaking waves. *J. Phys. Oceanogr.* **30**, 2404–2418.

ONORATO, M., CAVALERI, L., FOUQUES, S., GRAMSTAD, O., JANSSEN, P. A. E. M., MONBALIU, J., OSBORNE, A. R., PAKOZDI, C., SERIO, M., STANSBERG, C. T., TOFFOLI, A., & TRULSEN, K. 2009 Statistical properties of mechanically generated surface gravity waves: a laboratory experiment in a three-dimensional wave basin. *J. Fluid Mech.* **637**, 235–257.

ONORATO, M., OSBORNE, A. R. & SERIO, M. 2002 Extreme wave events in directional, random oceanic sea states. *Phys. Fluids* **14**, 25–28.

ONORATO, M., OSBORNE, A. R., SERIO, M. & BERTONE, S. 2001 Freak wave in random oceanic sea states. *Phys. Rev. Lett.* **86**, 5831–5834.

RAPP, R. J. & MELVILLE, W. K. 1990 Laboratory measurements of deep-water breaking waves. *Phil. Trans. R. Soc. Lond.* **A311**, 735–800.

TULIN, M. P. & WASEDA, T. 1999 Laboratory observations of wave group evolution, including breaking effects. *J. Fluid Mech.* **378**, 197–232.

WASEDA, T., KINOSHITA, T. & TAMURA H. 2009 Evolution of a random directional wave and freak wave occurrence. *J. Phys. Oceanogr.* **39**, 621–639.

WASEDA, T. & TULIN, M. P. 1999 Experimental study of the stability of deep-water wave trains including breaking effects. *J. Fluid Mech.* **401**, 55–84.

WATSON, K. M. & WEST B. J. 1975 A transport-equation description of nonlinear ocean surface wave interactions. *J. Fluid Mech.* **70**, 815–826.

WEST, B. J., BRUECKNER, K. A. & JANDA, R. S. 1987 A new numerical method for surface hydrodynamics. *J. Geophys. Res.* **C92**, 11803–11824.

YOUNG, I. R. & BABANIN, A. V. 2006 Spectral distribution of energy dissipation of wind-generated waves due to dominant wave breaking. *J. Phys. Oceanogr.* **36**, 376–394.